Supporting Information

Renvall and Hari 10.1073/pnas.0911265106

SI Text

Details on Experiments. All experiments were performed on two phantoms (uniform and gradient phantom) with a standard gradient recalled (GRE) echo planar imaging (EPI) pulse sequence on a 3-T whole body MRI scanner (Signa Excite 3.0T; GE Healthcare; software rev. E2.0_M4_0502.b), equipped with an eight-channel phased array head coil (Signa Excite). The field of view was 20 cm for the uniform and 19 cm for the gradient phantom. In all experiments, the image matrix was 64 × 64 voxels, slice thickness/gap between slices 3.0 mm/0.0 mm, flip angle 90°. Frequency was encoded from left to right. Other parameters, TR, TE, and number of time points were adjusted between measurements. The data from the first block of data (10 or 30 TRs) was discarded in each experiment to allow the longitudinal magnetization to reach pseudo steady state and to start from the beginning of a block.

The fMRI phantoms were made of 18.6-cm (uniform phantom) and 18.8-cm (gradient phantom) hollow acrylic cylinders of 16/20-mm inner/outer diameters. The cylinders were filled with ion-exchanged water and plugged with finger tips of a vinyl disposable glove. The coils, wound of 0.15-mm copper thread to the approximate center of the tube, were separated by 1.73 cm; this Maxwell's coil configuration aimed to produce a considerably homogeneous field or linear gradient field for the uniform phantom and the gradient phantom, respectively. In the uniform phantom, the pair of coils was wound in the same direction so that both coils induced positive B_z; in the gradient phantom the directions of the coils were opposite, so that one of the coils induced positive B_z and the other negative.

As the coils were wound of a single contiguous thread in each phantom, the wire went twice between the coils for length of the 1.73-cm separating distance (Fig. 1*A*); those parts were aligned parallel to the tube's central axis. From the tubes, the wires were twisted and led to the receiver device approximately perpendicularly to the direction of the main field of the magnet (z direction). The current in the coils surrounding the phantoms was controlled with Presentation software (version 12.0 Build 01.23.08; Neurobehavioral Systems) via a fiber-optic signal pathway. A receiver device, powered by a battery, controlled the electrical switching of the "stimulus periods" by opening and closing a logic gate between the lead ends of the coils; the duration of the stimulus periods was varied between 7.5 and 30 s (5 or 15 TRs). Only step-transition stimuli were applied.

The phantoms were positioned in the central region of the head coil, with the axes of the cylinders along the z direction. Coarse alignment was guided by the alignment lights of the scanner, and the alignments were improved by measuring the tubes' distances from the rails of the head coil to within 1 mm between two measurement locations ≈10 cm apart in each of the cases, thus the axes of the head coil and the phantoms were within 0.6° from each other. The two phantoms were scanned in successive sessions.

After each setup process, a localizer scan was acquired to verify the good alignment and serve as the base to place the slices for the rest of the measurements. During the localizer scans, the phantoms were in the activation condition, meaning that no current was applied to the coils.

Stacks of nine (five) transverse slices, perpendicular to the z direction, were assigned for the uniform (gradient) phantom. With the uniform phantom, the landmark set in the middle of the coils was used as the location of the middlemost slice. With the gradient phantom, the signal slightly decreased in the area between the coils and was used as the positioning reference. The region of interest was chosen from slice 5 for the uniform phantom (slice 2 for the gradient phantom), being thus the third (fourth) slice in the interleaved acquisition order and the scanning of the slice began after 2/9 (3/5) TRs, e.g., at 444 ms (1,200 ms) for TR = 2,000 ms. The step adjustment of the field was triggered by the excitation pulse of the first slice of the volume, and the delays of the system from triggers to stimuli were on the order of 10 ms. Settling times (time to reach step-transition amplitude) of the current in the Maxwell coils, measured outside the magnet environment, were <0.1 ms.

Details on Simulations. The simulations were carried out on a column of 22,001 discrete elements of length 1 μm and indefinite width, spanning 2.2 cm in the direction of the signal displacement (i.e., z-direction); the middlemost 3,000 elements thus depicted an ideal 3-mm-thick slice. The simulation included exciting the middlemost slice and the slices next to it at correct times.

Two apparent slice displacements, 150 and 300 μm, were applied. The choices were based on assuming that the blood volume occupied by red cells (hematocrit) is ≈45% and the modulation of the venous oxygenation 0.16 or, as percentage, 26% (1). Multiplying the displacement caused by the 10-μT modulation between completely oxygenated and oxygen-depleted erythrocytes by 7.2% (45% × 0.16) yields a displacement of 144 μm, which would relate to the changes of whole blood in veins, if only as an average.

Before excitations, the longitudinal magnetization available in each element $M_z(z, t)$ was evaluated on the basis of time elapsed after the previous simulated excitation ($t - t_-$) and the T_1 assigned for the sample:

$$M_z(z, t) = M_z(z, t_-) + (M_0 - M_z(z, t_-))(1 - \exp(-(t - t_-)/T_1)), \quad [1]$$

where z, t, M_0, and t_- are the z-coordinate of the element, time, magnetization in thermal equilibrium, and time of the previous evaluation of magnetization, respectively.

The power deposited in the proton population is a function of z and the slice profile. The effects of the excitation pulses were approximated by different slice profiles [($P(z)$, normalized between 0 and 1], with maximum intensity corresponding to a 90° flip angle, which determined how much longitudinal magnetization was transferred to the excited pool. The transverse magnetization was then calculated as

$$M_{xy} = \sum_k M_z(k, t)\sin(\pi/2 \cdot P(k)). \quad [2]$$

Sigmoid curves were used to link zero-level power to a constant power in $P(z)$. The widths of the sigmoid curves were varied to simulate different excitation pulse profiles, and the nominal slice thickness (3 mm) in the simulations was defined as the full width at half maximum of the profile. The new longitudinal magnetization value was recorded so that it could be used in the following simulation step. The signal was stored in the case of the middlemost slice.

Perfect spoiling of transverse magnetization between excitations was assumed, i.e., the signal was supposed to emerge only from the newly excited magnetization. Transverse relaxation was omitted as it plays no fundamental role in the proposed mechanism of transient generation. A flowchart of the simulation is shown in Fig. S1.

Fig. S2 illustrates the signal acquired in the simulations. Here, the longitudinal magnetization immediately before an excitation was used as the pool of excitable spins. The excitation of the indicated slice profiles and locations yielded the postexcitation longitudinal magnetization; the signal was calculated from the difference of the preexcitation and postexcitation longitudinal magnetizations according to Eq. **2**.

In Fig. S3, the flip angle was varied between acquisitions. Reducing the flip angle made the transients weaker.

1. Lu H, van Zijl PCM (2005) Experimental measurement of extravascular parenchymal BOLD effects and tissue oxygen extraction fractions using multi-echo VASO fMRI at 1.5 and 3.0 T. *Magn Reson Med* 53:808–816.

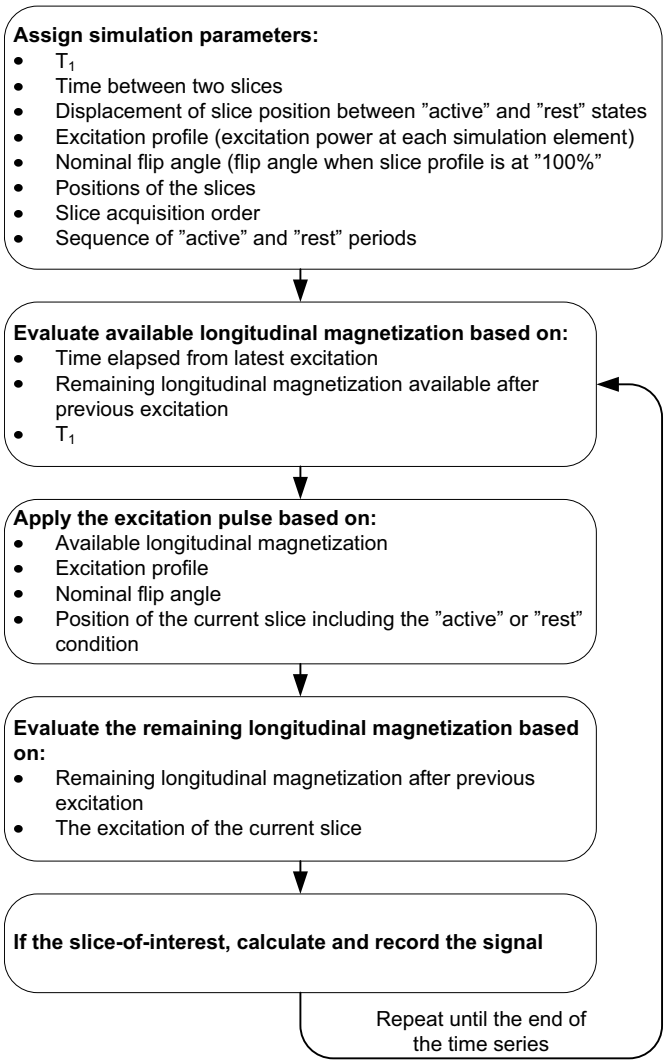

Fig. S1. Simulation flowchart.

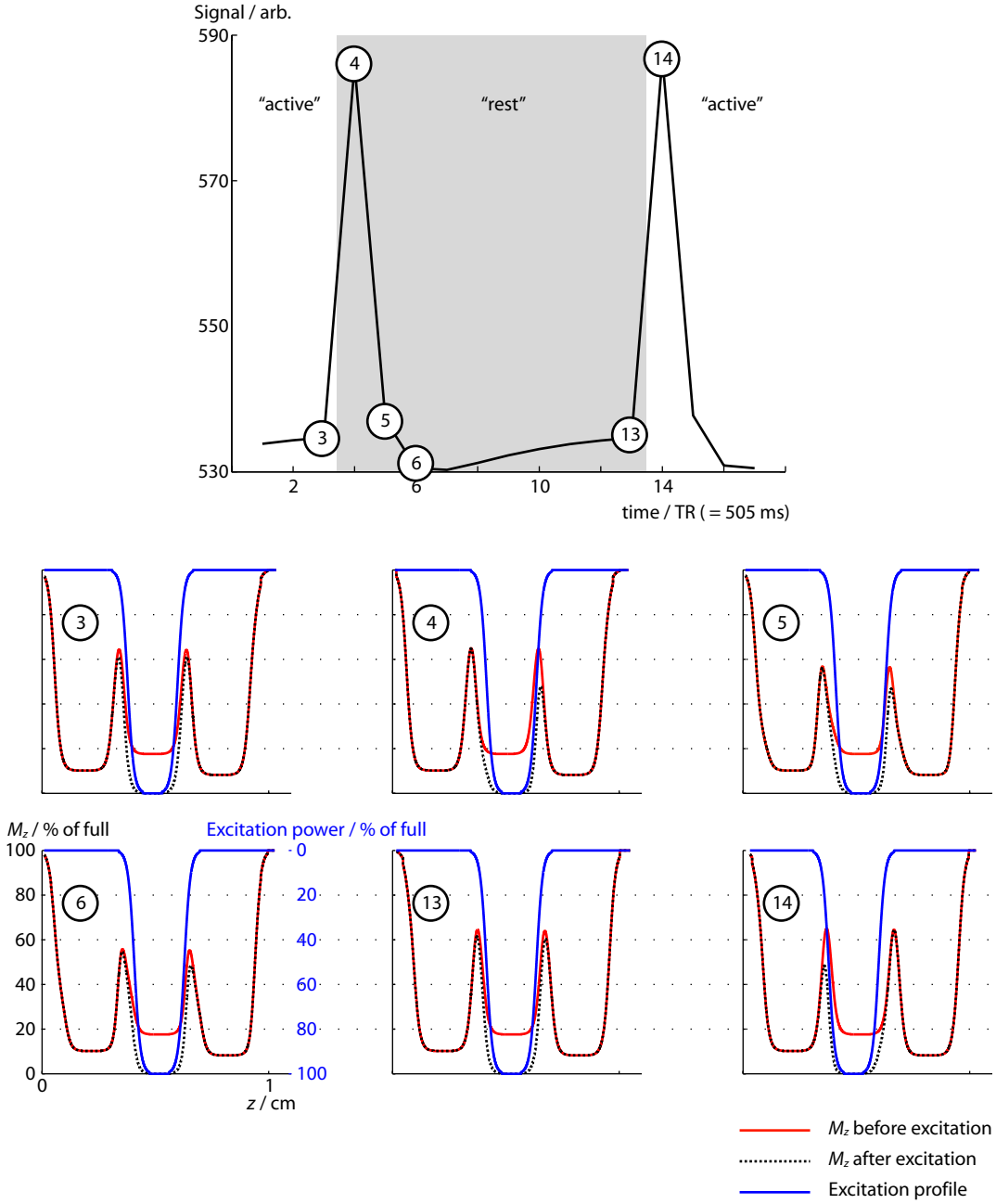

Fig. S2. A simulation of the emergence of the transient from slice misplacements over time. The simulation consists of exciting three adjacent slices in an interleaved manner. The top panel shows the obtained transient. The other panels (labeled 3, 4, 5, 6, 13, and 14, and referring to corresponding time points in the top panel) show the longitudinal magnetization (M_z) immediately before (solid red lines) and after (dotted black lines) the excitation of the middlemost slice (blue lines; for scale, see the right-hand side of panel 6). Note that in panels 4 and 14, M_z is symmmetric before the excitation (red line), but strongly asymmetric after the excitation (dashed line), because of the location of the excitation profile (blue line). Instead in e.g., panel 3, M_z is symmetric both before and after the excitation. The asymmetry in panels 4 and 14 arises from slice selection that targeted the sample in a location where M_z had initially relaxed more than for instance in panel 3. At time point 6, the longitudinal magnetization available for the excitation is less than at point 13, for instance, because the excitations of the adjacent slices have targeted the edges of those slices (overlapping with the middlemost slice) with more power than previously (visible as the different amplitudes of the M_z traces). As time elapses, the system resumes the pseudo steady state once more (as in 13).

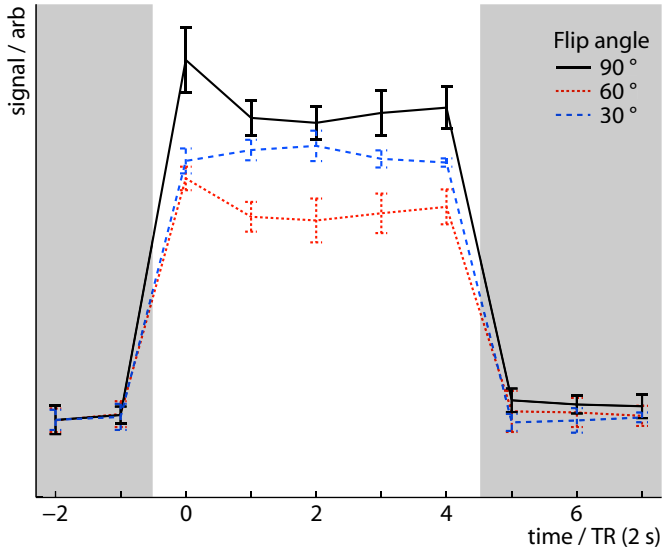

Fig. S3. Reducing flip angle suppressed transients. The gradient phantom was used while scanning seven times a sequence consisting of five time points at both active and rest conditions. The signals are from slice 3/9 of an interleaved acquisition with TR = 2 s, TE = 40 ms, field of view = 19 cm, slice thickness = 3 mm, no gap between slices, 3 × 3-voxel region-of-interest in the middle of the phantom of an image matrix of 64 × 64, and the flip angle as indicated. The scale is the same for all plots, the vertical axis spans 120 units in the image scale. Error bars indicate the standard deviation at each time point.